Research Square

Preprints are preliminary reports that have not undergone peer review.
They should not be considered conclusive, used to inform clinical practice,
or referenced by the media as validated information.

High-capacity uranium extraction from seawater through constructing synergistic multiple dynamic bonds in confined spaces

Guangshan Zhu

zhugs@nenu.edu.cn

Key Laboratory of Polyoxometalate and Reticular Material Chemistry of Ministry of Education

Ye Yuan

Key Laboratory of Polyoxometalate and Reticular Material Chemistry of Ministry of Education, Faculty of Chemistry, Northeast Normal University

Doudou Cao

Key Laboratory of Polyoxometalate Science of the Ministry of Education, Faculty of Chemistry, Northeast Normal University

Cui Fengchao

Key Laboratory of Polyoxometalate Science of the Ministry of Education, Faculty of Chemistry, Northeast Normal University

Cheng Zhang

Key Laboratory of Polyoxometalate Science of the Ministry of Education, Faculty of Chemistry, Northeast Normal University

Yajie Yang

Key Laboratory of Automobile Materials of Ministry of Education & School of Materials Science and Engineering, Jilin University

Yingbo Song

Key Laboratory of Polyoxometalate Science of the Ministry of Education, Faculty of Chemistry, Northeast Normal University

Jiarui Cao

Key Laboratory of Polyoxometalate Science of the Ministry of Education, Faculty of Chemistry, Northeast Normal University

Yue Zheng

Key Laboratory of Polyoxometalate Science of the Ministry of Education, Faculty of Chemistry, Northeast Normal University

Shusen Chen

Beijing Research Institute of Chemical Engineering and Metallurgy, CNNC Key Laboratory on Uranium Extraction from Seawater,

Yan Song
Beijing Research Institute of Chemical Engineering and Metallurgy, CNNC Key Laboratory on Uranium Extraction from Seawater,
Fengju Wang
Beijing Research Institute of Chemical Engineering and Metallurgy, CNNC Key Laboratory on Uranium Extraction from Seawater,

---

Article

Keywords:

Posted Date: March 18th, 2024

DOI: https://doi.org/10.21203/rs.3.rs-4038599/v1

License: This work is licensed under a Creative Commons Attribution 4.0 International License.
Read Full License

Additional Declarations: There is **NO** Competing Interest.

Version of Record: A version of this preprint was published at Nature Water on January 2nd, 2025. See the published version at https://doi.org/10.1038/s44221-024-00346-y.

High-capacity uranium extraction from seawater through constructing synergistic multiple dynamic bonds in confined spaces

Seawater is the largest uranium reserve in the world, and the efficient extraction of uranium from seawater facilitates the sustainable development of the nuclear industry for thousands of years. However, conventional extraction processes must suffer the dissociation of CO_3^{2-} ions from $[UO_2(CO_3)_3]^{4-}$ anions to bind the uranyl core, which has a high energy barrier, resulting in the poor selectivity and long working times. Here, we combine a molecular templating strategy to synthesize five hydroxy-rich covalent organic frameworks (COFs) with tunable nanopore sizes (from 0.6 to 2.5 nm). In the 1.1-nm-sized COF cavity, hydroxyl groups coupled with the hydrogen-bonded NH_4^+ cations selectively bind uranyl tricarbonate ions *via* synergistic electrostatic and hydrogen-bonding interactions. This framework exhibits high uranium-extraction capability with a removal ratio of >99.99 % in 400 min. Notably, a record uranium-adsorption uptake is achieved with a capacity of 23.68 mg g^{-1} in 7 days from natural seawater, surpassing that of classical amidoxime-based adsorbents by a factor of 350%.

According to the United Nations Framework Convention on Climate Change (UNFCCC), more than 20 countries have called for increasing the global nuclear power capacity to three times its 2020 level by 2050[1]. Uranium fission power, currently the only controllable nuclear energy, would be developed at a high speed because of the carbon emission-free and high energy production[2]. Consequently, the stable smelting and production of raw uranium minerals will be

under unprecedented pressure for the sustainable development of nuclear power industries in the next few decades[3]. Seawater contains the largest uranium reserve ~4.5 billion tons, a potentially enormous resource that could support nuclear energy production for thousands of years[4,5]. Nevertheless, the concentration of uranium in the ocean is extremely low (~3.3 ppb) and it coexists with numerous interfering ions at high concentrations[6]. In the past several decades, various methods have been developed for extracting uranium from seawater, including electrocatalytic reduction, photocatalytic reduction, and adsorption[7–9]. Among these methods, adsorption is the most promising route for the industrialized extraction of uranium from seawater because of its simple operation and low energy consumption[10]. However, current adsorbents extract uranyl ions through coordination bonding, falling short of the targets for practical utilization in capacity, selectivity, and working time[11].

Natural seawater is weakly alkaline with a pH of 7.5−8.3, containing 1.6−2.5 mmol L^{-1} carbonate ions, where uranium(VI) combines with three carbonate (CO_3^{2-}) ions to form stable uranyl tricarbonate anions ($[UO_2(CO_3)_3]^{4-}$)[12,13]. In conventional extraction processes, $[UO_2(CO_3)_3]^{4-}$ anions first undergo the dissociation of CO_3^{2-} ions, and then, the binding group (e.g., amidoxime, phosphoric acid, *o*-diphenol, *etc*.) coordinates to the exposed uranyl center for its capture[14–18]. This dissociation step has a high energy barrier, resulting in the inability of most adsorption groups to strip the carbonate ion from the uranyl ion. Currently, the amidoxime group is widely used, which has a binding energy of −4.1 kcal mol^{-1} in the form of η2-N, O with the uranyl ion, slightly higher than that of CO_3^{2-} ion (binding energy −2.9 kcal mol^{-1})[19,20]. However, amidoxime groups preferentially bind iron and vanadium ions in seawater, and the slow dissociation kinetics of CO_3^{2-} ions from uranyl tricarbonate prolong the adsorption time. These poor selectivity and long working times are disadvantages for the industrialization of uranium

extraction from seawater[21–23]. Directly binding $[UO_2(CO_3)_3]^{4-}$ anions from seawater to avoid the slow dissociation process is an effective approach to achieve rapid speed and high capacity for uranium extraction; however, this work is still in the initial stage.

Herein, trimesic acid was selected as the template of $[UO_2(CO_3)_3]^{4-}$ anion due to the similar equatorial dimension, and the $[UO_2(CO_3)_3]^{4-}$ anion imprinted complex composed of trimesic acid and three glycidol molecules was decorated on COF channels. Accordingly, five covalent organic framework (COF) materials were synthesized with the same *hcb* topology, abundant hydroxyl groups, and a pore size ranging from 0.64 to 2.5 nm. In the nano-sized confinement space, the electronegative –OH groups on the COF channel stabilize cations through electrostatic interactions, forming $[UO_2(CO_3)_3]^{4-}$ anion-specific nanofluidic channels. After that, the $[UO_2(CO_3)_3]^{4-}$ anion sticks close to NH_4^+ cations to obtain a stable anion–cation equilibrium while forming multiple hydrogen-bonding interactions with the COF fragment. These synergistic multiple dynamic bonds captured $[UO_2(CO_3)_3]^{4-}$ anions selectively, achieving a high uranium uptake capacity of 23.68 mg g^{-1} in 7 days from natural seawater. This study reports an effective strategy for constructing synergistic multiple dynamic bonds in the COF nanocavity to realize the rapid adsorption and high capacity for real-world uranium extraction.

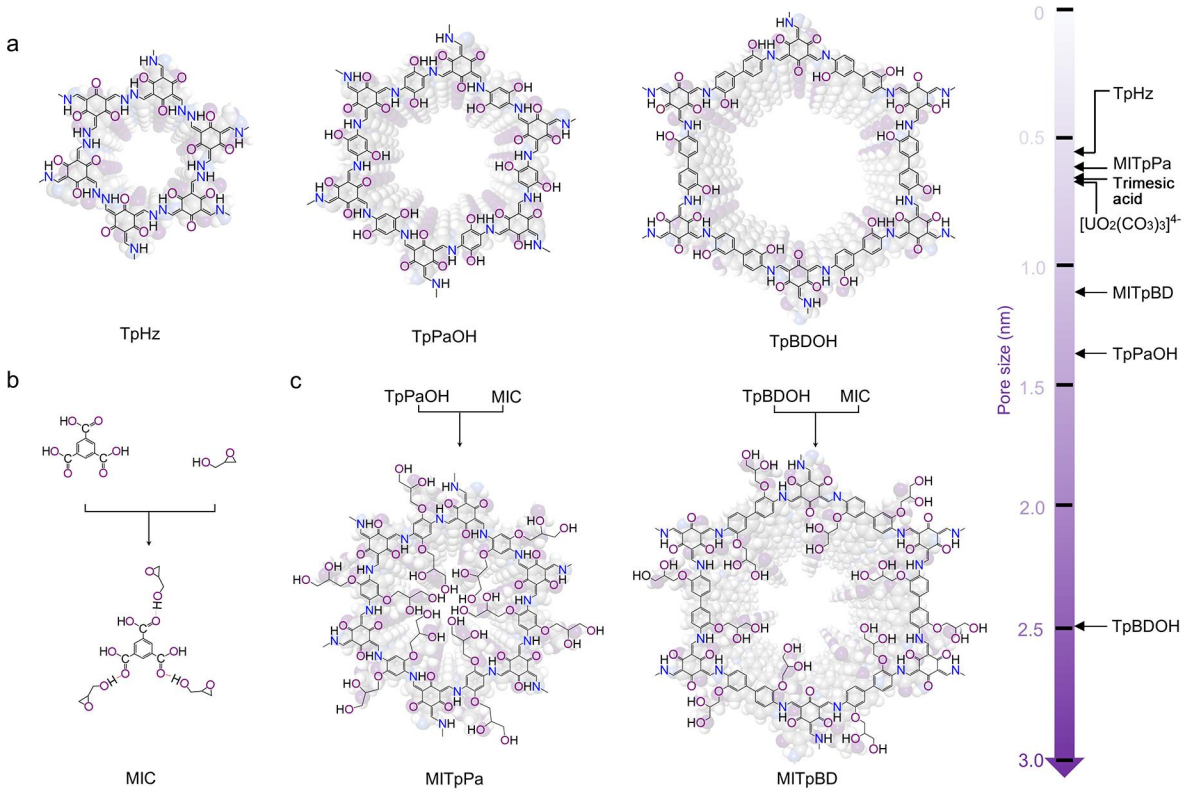


Fig. 1 | Schematic representation of hydroxy-rich COF networks. a, Three COF solids (i.e., TpHz, TpPaOH, and TpBDOH) synthesized by solvothermal method.[24–26] **b,** Trimesic acid as the template to form the $[UO_2(CO_3)_3]^{4-}$ anion imprinted complex (MIC). **c,** Pyrolysis of epoxy to synthesize the $[UO_2(CO_3)_3]^{4-}$ anion imprinted COF networks, MITpPa and MITpBD.

Results and discussion

Structural analysis of hydroxy-rich COFs.

In the uranyl tricarbonate ion ($[UO_2(CO_3)_3]^{4-}$), the uranium center forms axial double bonds with two oxygen atoms and coordinates to six oxygen atoms from three carbonate ions in the equatorial region; it has an axial dimension of 3.7 Å and an equatorial dimension of 7.2 Å (Fig. 1). To construct an ideal binding cavity for uranyl tricarbonate ions, hydrazine hydrate (Hz), 2,5-diaminobenzene-1,4-diol dihydrochloride (PaOH), and 3,3-dihydroxybenzidine (BDOH) together with 1,3,5-triformyl chloroquinone (Tp) were degassed with three freeze–pump–thaw

cycles and heated at 393 K for 72 h to synthesize COF networks, named TpHZ, TpPaOH, and TpBDOH, respectively (Supplementary Fig. 1). Fourier transform infrared (FT-IR) spectra of TpHZ, TpPaOH, and TpBDOH exhibit several characteristic peaks of C=O (1582 cm^{-1}), C=C (1580 cm^{-1}), and C–N (1275 cm^{-1}), which confirm the formation of the proposed β-ketoenamine–linked structure (Supplementary Figs. 2–4). Meanwhile, a series of diffraction peaks are observed in the powder X-ray diffraction (PXRD) patterns of TpHz (θ = 6.8°, 11.5°, and 27.2°), TpPaOH (θ = 4.6° and 26.7°), and TpBDOH (θ = 3.4°, 5.8°, and 26.3°), which demonstrate the eclipsed AA-stacking mode of COF layers (Supplementary Figs. 5–7)[24–26].

Trimesic acid with an equatorial dimension (7.0 Å) similar to $[UO_2(CO_3)_3]^{4-}$ ions was selected as the template for constructing the $[UO_2(CO_3)_3]^{4-}$ anion–imprinted sites in the porous architecture. The molecularly imprinted complex (MIC) was obtained as a white powder by reacting trimesic acid with 3 equiv. of glycidol. In the FT-IR spectrum of glycidol, the absorption peaks at 3393 and 1040 cm^{-1} correspond to –OH and C–O–C groups, respectively. For that of trimesic acid, the infrared absorption peak at 1624 cm^{-1} is ascribed to the –COOH segment. After the MIC is formed, the peaks of –OH and –COOH shift to 3618 and 1612 cm^{-1}, respectively, proving the formation of hydrogen bonds between the –COOH groups of trimesic acid and the –OH groups of glycidol (Supplementary Figs. 8 and 9)[27–29]. Then, the MIC was decorated on the COF networks (TpPaOH and TpBDOH, respectively) via the solvothermal reaction in ethanol at 353 K for 24 h. Washing three times with ethanol, trimesic acid templates were leached out from the porous architecture to obtain $[UO_2(CO_3)_3]^{4-}$ anion imprinted COF networks, named MITpPa and MITpBD (from TpPaOH and TpBDOH, respectively). Compared to the FT-IR spectra of TpPaOH and TpBDOH, the IR absorption peak at 1040 cm^{-1}, assigned to the C–O–C group, in the FT-IR spectra of MITpPa and MITpBD, confirms the successful

decoration of glycidol on COF structures. Meanwhile, the new signal peaks at ~73, ~70, and ~64 ppm in solid-state ^{13}C nuclear magnetic resonance (NMR) spectra of MITpPa and MITpBD (Fig. 2a) correspond to carbon atoms of glycidol fragment[30]. The PXRD pattern of MITpPa exhibits peaks centered at 2θ = 4.6 and 26.7°, corresponding to the (100) and (001) crystal planes, respectively; and the PXRD pattern of MITpBD exhibits peaks centered at 2θ = 3.4, 5.8, and 26.7°, corresponding to the (100), (110), and (001) crystal planes, respectively, indicating the high crystallinity of $[UO_2(CO_3)_3]^{4-}$ anion imprinted COF networks (Fig. 2b)[24–26].

According to N_2 sorption experiments, all COF materials exhibit type I reversible isotherms, indicating their microporous characteristic (Fig. 2c,d)[26]. Brunauer–Emmett–Teller (BET) analysis shows that the specific surface areas of TpHz, TpPaOH, and TpBDOH are 277.2, 304.5, and 443.6 $m^2\ g^{-1}$, respectively; interpreted by nonlocal density functional theory (NL-DFT), the pore size distributions are centered at 0.6 (TpHz), 1.4 (TpPaOH), and 2.5 nm (TpBDOH), respectively (Supplementary Table 1). After grafting the imprinted sites, the BET surface areas of MITpPa and MITpBD decrease to 188.3 and 233.6 $m^2\ g^{-1}$, respectively. These changes are attributed to glycidol fragments occupying the pore channels of TpPaOH and TpBDOH and increasing the mass per unit, suggesting the successful grafting of glycidol groups within COF channels. The grafting amounts in MITpPa and MITpBD are 61% and 60%, respectively, as analyzed by elemental content analysis. An estimation of the electrostatic potential (ESP) of COF materials shows that the –OH groups on glycidol fragments possess the minimum ESP values, where the electronegative oxygen atoms can stabilize cations via electrostatic interactions (Fig. 2e)[31].

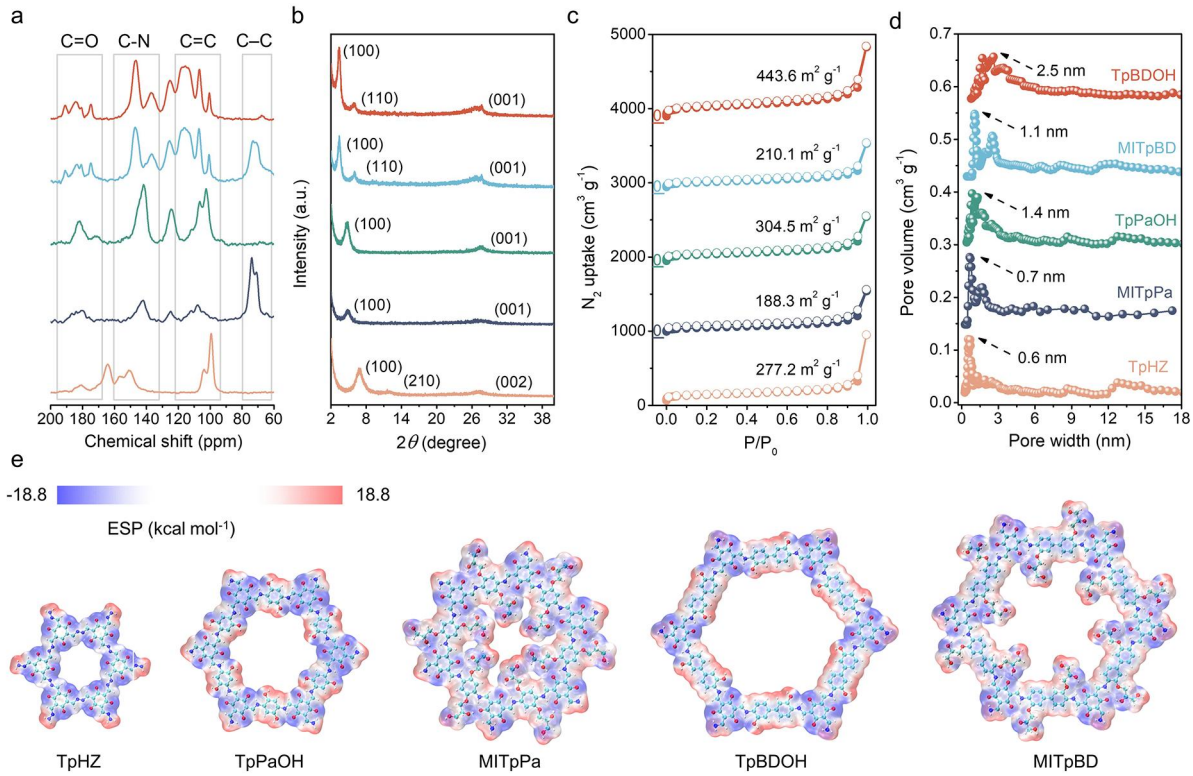


Fig. 2 | Structures and pore environments. a, Solid-state ^{13}C CP/MAS NMR spectra; **b,** PXRD patterns; **c,** nitrogen adsorption isotherms; **d,** pore size distributions; **e,** ESP distribution maps of TpHz, MITpPa, TpPaOH, MITpBD, and TpBDOH, respectively.

Uranium uptake in hydroxy-rich COFs.

The ion uptake capacity of hydroxy-rich COFs was studied by mixing 5 mg of COF powder in an ammonium uranyl tricarbonate solution (500 mL, ~10 ppm) at 298 K and pH = 8–9. As shown in Fig. 3a and Supplementary Table 2, the adsorption uptakes of TpHz, TpPaOH, and TpBDOH for $[UO_2(CO_3)_3]^{4-}$ anions are 11.2, 86.7, and 55.7 mg g^{-1}, respectively. After grafting the imprinted sites, the adsorption capacities of MITpPa and MITpBD for $[UO_2(CO_3)_3]^{4-}$ anions are 137.0 and 206.3 mg g^{-1}, respectively. Fitted by the *pseudo-second-order* kinetic model, the ion uptake

processes of these COFs are rate-limited by chemical adsorption (Supplementary Figs. 18–20 and Supplementary Tables 3 and 4)[32]. Time-course adsorption measurements indicate that MITpBD exhibits a uranium uptake of 142.5 mg g^{-1} in the first 60 min of contact (Fig. 3a), which is the highest value achieved among all adsorbents reported for $[UO_2(CO_3)_3]^{4-}$ anion adsorption (~10 ppm; Fig. 3b and Supplementary Table 7).

The adsorption thermodynamics of COF samples were collected at 298 K by exposing the samples to ammonium uranyl tricarbonate solutions with concentrations in the range of 1–150 ppm (pH = 8–9). Fitted by the *Langmuir* model, the saturation capacities of TpPaOH, TpBDOH, MITpPa, and MITpBD are 175.0, 203.3, 486.0, and 800.0 mg g^{-1}, respectively (Fig. 3c, Supplementary Figs. 21–23, and Supplementary Tables 5 and 6). The binding affinity of all COF solids for $[UO_2(CO_3)_3]^{4-}$ anions was calculated by impregnating 10 mg of the COF powder into 300 mL of the 5 ppm ammonium uranyl tricarbonate solution at 298 K and pH = 8–9. After reacting the solution for 400 min, the final concentrations of solutions are 0.4 (MITpBD), 1.6 (MITpPa), 617.0 (TpBDOH), and 817.3 (TpPaOH) ppb, corresponding to the removal ratios of 99.99%, 99.97%, 87.29%, and 83.66%, respectively. The distribution coefficient (K_d) of MITpBD is 3.75×10^8 (Fig. 3d), which is higher than those of classical uranium adsorbents, including PPA@MISS-PAF-1 (2.2×10^7)[10], MISS-PAF-1 (1.4×10^7)[10], ZP-PAN (7.4×10^6)[33], and SMON-PAO (3.8×10^5)[34] (Fig. 3e,f and Supplementary Table 8).

Ion selectivity experiments of the MITpBD adsorbent were performed in uranium-spiked seawater (3 ppm) containing different competing cations, i.e., Na^+, K^+, VO_2^+, Mg^{2+}, Ca^{2+}, Cd^{2+}, Ni^{2+}, Cu^{2+}, Zn^{2+}, and Fe^{3+} (pH = 8–9). As shown in Fig. 3g, the uranium uptake of MITpBD is 65.3 mg g^{-1} with a selectivity coefficient (mass ratio of the U and M capacities) of >69.9 for $[UO_2(CO_3)_3]^{4-}/VO_2^+$ (Supplementary Fig. 24). Furthermore, different competing anions

including 3 ppm $[UO_2(CO_3)_3]^{4-}$, NO_3^-, SO_4^{2-}, HPO_4^{2-}, Br^-, I^-, and F^- were added to the solution to tested the selective uptake of the COF sample. As shown in Supplementary Fig. 25, the uranium uptake capacity of MITpBD is ~60.8 mg g^{-1} in the presence of F^-, Br^-, I^-, NO_3^-, SO_4^{2-}, and HPO_4^{2-} indicating that these anions have little effect on the uranium uptake. To the best of our knowledge, the saturated adsorption capacity of MITpBD for $[UO_2(CO_3)_3]^{4-}$ anions is higher than that of all reported adsorbents for $[UO_2(CO_3)_3]^{4-}$ anions, including Ti_3C_2-AO-PA (108.5 mg g^{-1})[35], Ti_3C_2-AO (70.9 mg g^{-1})[35], and COF-DG (65.4 mg g^{-1})[36] (Fig. 3h and Supplementary Table 9).

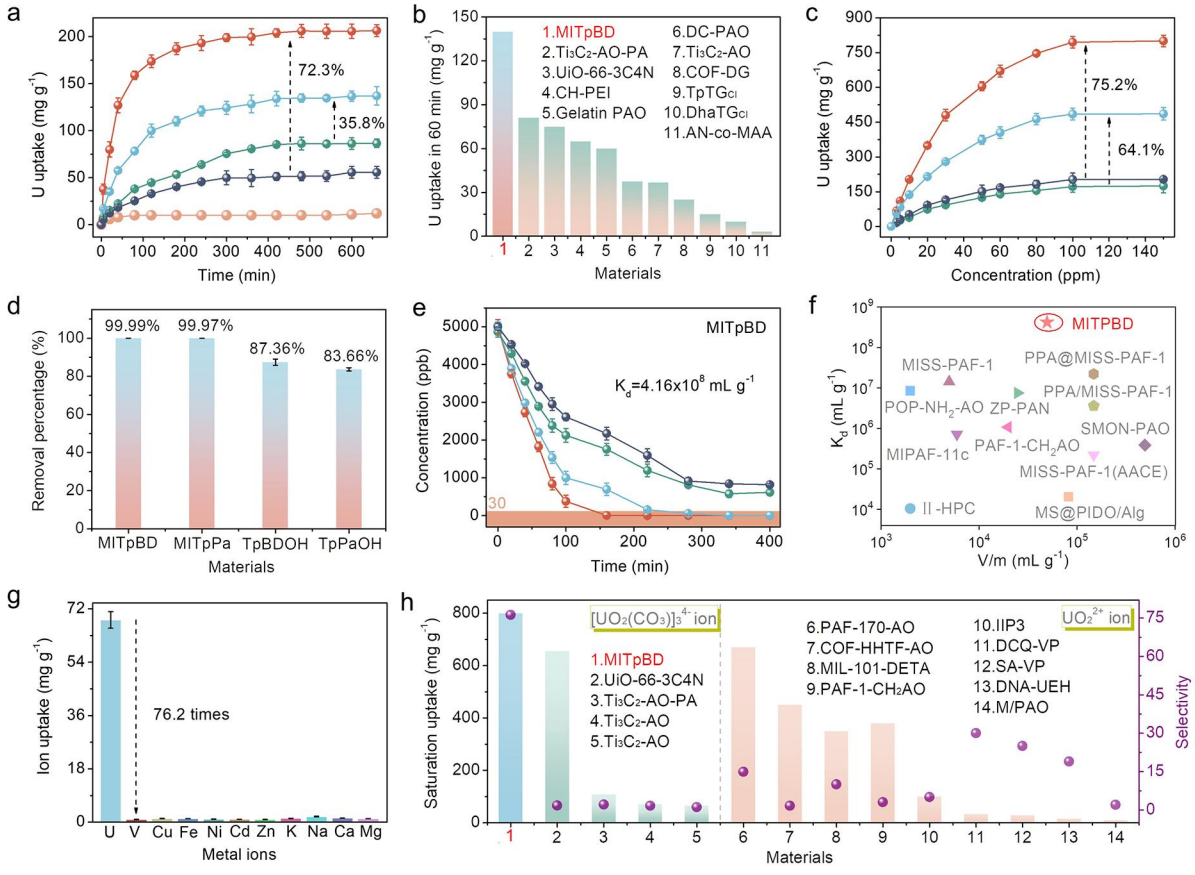


Fig. 3 | Ion uptakes of hydroxy-rich COFs. a, Uranium uptakes of different COFs at an initial uranium concentration of ~10 ppm (pH = 8–9). **b,** Comparison of $[UO_2(CO_3)_3]^{4-}$ adsorption rate of adsorbents under similar conditions (initial concentrations in the range of 6–10 ppm at pH =

8–9) in the first 60 min (Supplementary Table 7). **c,** Uranium uptake capacities of different COFs at initial uranium concentrations in the range of 1–150 ppm (pH = 8–9). **d** and **e,** Removal kinetics and capability of different COFs in a ~5 ppm uranium solution (pH = 8–9). **f,** Comparison of the distribution coefficient (K_d) against *V/m* of the classical adsorbents under similar conditions (initial concentrations in the range of 6–10 ppm at an ambient pH, Supplementary Table 8). **g,** Selectivity of MITpBD in uranium-spiked seawater (3 ppm) containing different competing cations. **h,** Comparison of the ion selectivity and saturation uptake of MITpBD with those of reported adsorbents (Supplementary Table 9).

Adsorption mechanism of $[UO_2(CO_3)_3]^{4-}$ anions on hydroxy-rich COFs.

X-ray photoelectron spectroscopy (XPS) reveals the high-resolution $U4f_{5/2}$ and $U4f_{7/2}$ peaks $[NH_4]_4[UO_2(CO_3)_3]$ with binding energies of 393.3 and 382.5 eV, respectively[16]. After adsorption experiments, these values shift to 393.0 and 382.0 eV in the XPS spectrum of $[UO_2(CO_3)_3]^{4-}$ anion–adsorbed MITpBD (Fig. 4a). In addition to the variation in the U4f signal, the O1s XPS spectrum of $[UO_2(CO_3)_3]^{4-}$ anion–adsorbed MITpBD shows an emerging peak for U=O at 531.4 eV and the N 1s XPS spectrum shows a new peak for NH_4^+ at 402.3 eV (Supplementary Figs. 26 and 27)[37–38]. These changes indicate that uranium species maintain their +6 valence state during the adsorption process but the existing environment changes. Then, the electronic absorption spectra of MITpBD were recorded before and after the adsorption of $[NH_4]_4[UO_2(CO_3)_3]$ (AUTC) (Fig. 4b). The absorption peak of $[UO_2(CO_3)_3]^{4-}$ anion–adsorbed MITpBD is considerably red-shifted compared to that of $[NH_4]_4[UO_2(CO_3)_3]$, confirming the charge transfer from $[NH_4]_4[UO_2(CO_3)_3]$ to the COF network[39].

To determine the binding pattern of uranium atoms, the adsorption mechanism was studied via stepwise adsorption experiments of NH_4^+ cations and $[UO_2(CO_3)_3]^{4-}$ anions. 5 mg of the

MITpBD powder was added to 500 mL of ammonium chloride solution (1 mol L^{-1}) at 298 K (named MITpBD@NH_4Cl). After stirring for 24 h, the filtrate was transferred to 500 mL of a 10 ppm sodium uranyl tricarbonate solution (SUTC) and stirred for 24 h, denoted as MITpBD@NH_4Cl@SUTC. FT-IR spectra show that the –NH stretching vibration peak shifts from 3018 to 2980 cm^{-1} and the –OH band shifts from 3399 to 3418 cm^{-1}, indicating the formation of hydrogen bonds between MITpBD and NH_4^+ cations[40]. After immersing the COF powder into a sodium uranyl tricarbonate solution, obvious changes are observed in the peaks of –NH (2980 to 2960 cm^{-1}) and –OH bands (3418 to 3240 cm^{-1}), confirming the electrostatic interaction between $[UO_2(CO_3)_3]^{4-}$ and NH_4^+ ions (Supplementary Fig. 32). Meanwhile, solid-state ^{15}N and ^{13}C NMR spectra were conducted for NH_4Cl, MITpBD@NH_4Cl, and MITpBD@NH_4Cl@SUTC (Fig. 4c,d). As shown in ^{15}N NMR spectra, the NH_4Cl signal shifts from −340.6 (pure NH_4Cl) to −357.5 ppm (MITpBD@NH_4Cl) because the electrically deficient N atom of NH_4^+ cations attracts the electron cloud of electronegative O atoms in the MITpBD network. After $[UO_2(CO_3)_3]^{4-}$ anions are adsorbed on MITpBD@NH_4Cl, the ^{15}N peak shifts from −357.5 to −361.2 ppm because the positive NH_4^+ cation further attracts the electron cloud of the $[UO_2(CO_3)_3]^{4-}$ anion via electrostatic interactions[41–42]. As shown in Fig. 4d, the solid-state ^{13}C NMR spectra reveal that the peaks of glycidol carbons shift from 70.18 to 70.51 ppm (C1) and 73.04 to 73.56 ppm (C2) after NH_4^+ cations are adsorbed on MITpBD. This phenomenon is attributed to that the interaction between the O atom of the –OH group and NH_4^+ cations decreases the electron cloud of the –OH group and increases the chemical shift of carbon atoms. After MITpBD@NH_4Cl combines with $[UO_2(CO_3)_3]^{4-}$ anions, this anion provides electrons to NH_4^+ cations and increases the electron cloud of the –OH group, decreasing the chemical shift of carbon atoms from 70.51 to 70.08 ppm for C1 and 73.56 to 73.12 ppm for C2 (Fig. 4d)[43].

DFT calculations were performed to confirm the configurations of COF unit cells with $[NH_4]_4[UO_2(CO_3)_3]$. The interaction energies of $[NH_4]_4[UO_2(CO_3)_3]$ with unit cells of different COFs follow the order of MITpBD, MITpPa, TpBDOH, and TpPaOH (Fig. 4g, Supplementary Figs. 40–44, and Supplementary Table 11). A comparison of the total interaction energies of MITpBD with NH_4^+ and $[UO_2(CO_3)_3]^{4-}$ shows that the COF fragment preferentially binds to NH_4^+ cations by forming a hydrogen bond between the –OH group of glycidol segments and N–H unit (Supplementary Fig. 45 and Supplementary Table 12). After incorporating $[UO_2(CO_3)_3]^{4-}$ anions inside the pores of MITpBD@NH_4Cl, the $[UO_2(CO_3)_3]^{4-}$ anion in the optimized structure sticks close to NH_4^+ cations to obtain a stable anion–cation equilibrium while forming multiple hydrogen-bonding interactions with the COF fragment. Because MITpBD possesses a more suitable pore size (1.1 nm), it forms at least triple hydrogen bonds with $[NH_4]_4[UO_2(CO_3)_3]$ and generates a stable conformation compared with other COF materials. The bond lengths of U=O and U–O are 1.82 and 2.56 Å in $[NH_4]_4[UO_2(CO_3)_3]$–adsorbed MITpBD, respectively, which are different from those of ammonium uranyl tricarbonate (1.81 Å for U=O and 2.44 Å for U–O; Fig. 4f and Supplementary Figs. 46 and 47). The increased U–O bond lengths coupled with the unchanged U=O bond length indicate that the –OH group and NH_4^+ cation form hydrogen bonds with O atoms on the equatorial plane of $[UO_2(CO_3)_3]^{4-}$ anions.

Further, the $[NH_4]_4[UO_2(CO_3)_3]$–adsorbed MITpBD was analyzed via extended X-ray absorption fine structure (EXAFS) spectroscopy (Fig. 4e and Supplementary Fig. 48). EXAFS analysis reveals that two axial oxygens and addition six coordination oxygens interact with the uranium center, consistent with the theoretical coordination number between uranium and oxygen atoms. The experimental bond distances of U=O (~1.82 Å) and U–O (~2.56 Å) bonds are consistent with those of DFT calculations (Fig. 4f and Supplementary Table 14). Therefore, the

adsorption mechanism of $[NH_4]_4[UO_2(CO_3)_3]$ on MITpBD is as follows: first, NH_4^+ cations form hydrogen bonds with the hydroxyl group of MITpBD. Then, NH_4^+ ions and –OH groups synergistically stabilize $[UO_2(CO_3)_3]^{4-}$ anions via electrostatic attraction and hydrogen bonding.

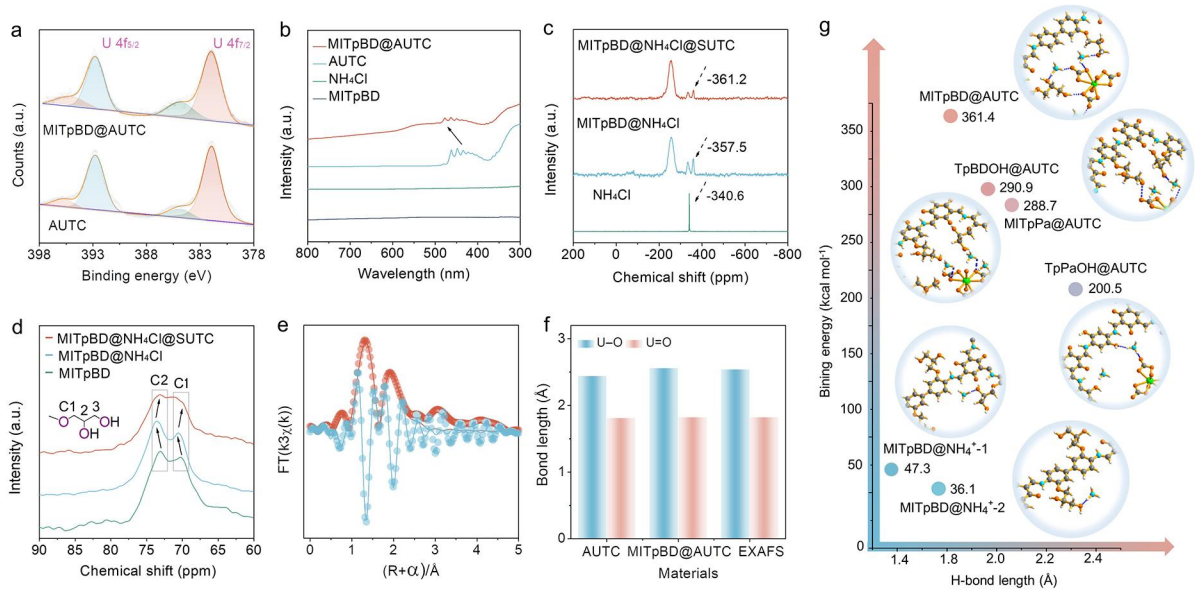


Fig. 4 | Uranium adsorption mechanism. a, U_{4f} XPS spectra of AUTC and MITpBD@AUTC. **b,** Solid-state electronic absorption spectra of MITpBD, NH_4Cl, AUTC, and MITpBD@AUTC. **c,** Solid-state ^{15}N CP/MAS NMR spectra of NH_4Cl, MITpBD@NH_4Cl, and MITpBD@NH_4Cl@SUTC. **d,** Solid-state ^{13}C CP/MAS NMR spectra of MITpBD, MITpBD@NH_4Cl, and MITpBD@NH_4Cl@SUTC. **e,** U LIII−edge EXAFS *R*−space and corresponding fitting curves of MITpBD@AUTC. The orange and blue lines represent *R*-space |χ(R)| and IM|χ(R)|, respectively. **f,** Comparison of the bond lengths between AUTC and MITpBD@AUTC, and EXAFS experimental results. **g,** DFT calculations of the binding energies of MITpBD@NH_4^+-1 (hydrogen bond between NH_4^+ and inner oxygen of glycidol fragment), MITpBD@NH_4^+-2 (hydrogen bond between NH_4^+ and outer oxygen of glycidol fragment), TpPaOH@AUTC, MITpPa@AUTC, TpBDOH@AUTC, and MITpBD@AUTC (Supplementary

Figs. 39–45). AUTC and SUTC are short for ammonium uranyl tricarbonate and sodium uranyl tricarbonate, respectively.

Recovery of extracted uranium

Five mg of the MITpBD powder was soaked in 500 mL (10 ppm, pH = 8−9) of an ammonium uranyl tricarbonate solution to obtain the $[UO_2(CO_3)_3]^{4-}$ anion–adsorbed MITpBD. Over ninety-nine percent of uranium ions were eluted by washing MITpBD with 30 mL of a 0.1 M Na_2CO_3 solution for 10 minutes and repeating the process three times. After treating at 373 K for 10 h, the thermally activated COF powder could be used in the next $[UO_2(CO_3)_3]^{4-}$ anion recovery cycle. Even after 18 cycles, the adsorption efficiency of MITpBD was more than 90% (Fig. 5a).

Uranium uptake in real seawater.

The adsorption uptake of MITpBD for uranium was tested in 100 L of real seawater (the concentration of uranium species in the Bohai Sea of China is ~3.4 ppb). As shown in Fig. 5b, the uranium uptake of MITpBD increases linearly with increasing adsorption time and the uranium capacity is 23.68 mg g^{-1} during 7 days of testing. MITpBD gives the highest uranium adsorption capacity from natural seawater among all adsorbents reported to date, including $[NH_4]^+[COF\text{-}SO_3^-]$ (17.8 mg g^{-1} in 7 days)[44], AO-OpNpNc (17.6 mg g^{-1} in 30 days)[45], and SSUP (12.3 mg g^{-1} in 3.5 days)[46]. Notably, this uptake capacity is at least 3.5 times higher than those of the previously reported adsorbent materials for $[UO_2(CO_3)_3]^{4-}$ anions, such as UiO-66-3C4N[47] (6.85 mg g^{-1} in 32 days), DC-PAO[48] (6.42 mg g^{-1} in 7 days), BD-TANO (5.92 mg g^{-1} in 30 days)[49], and crab carapaces (1.38 mg g^{-1} in 36 days)[50] (Fig. 5c and Supplementary Table 13).

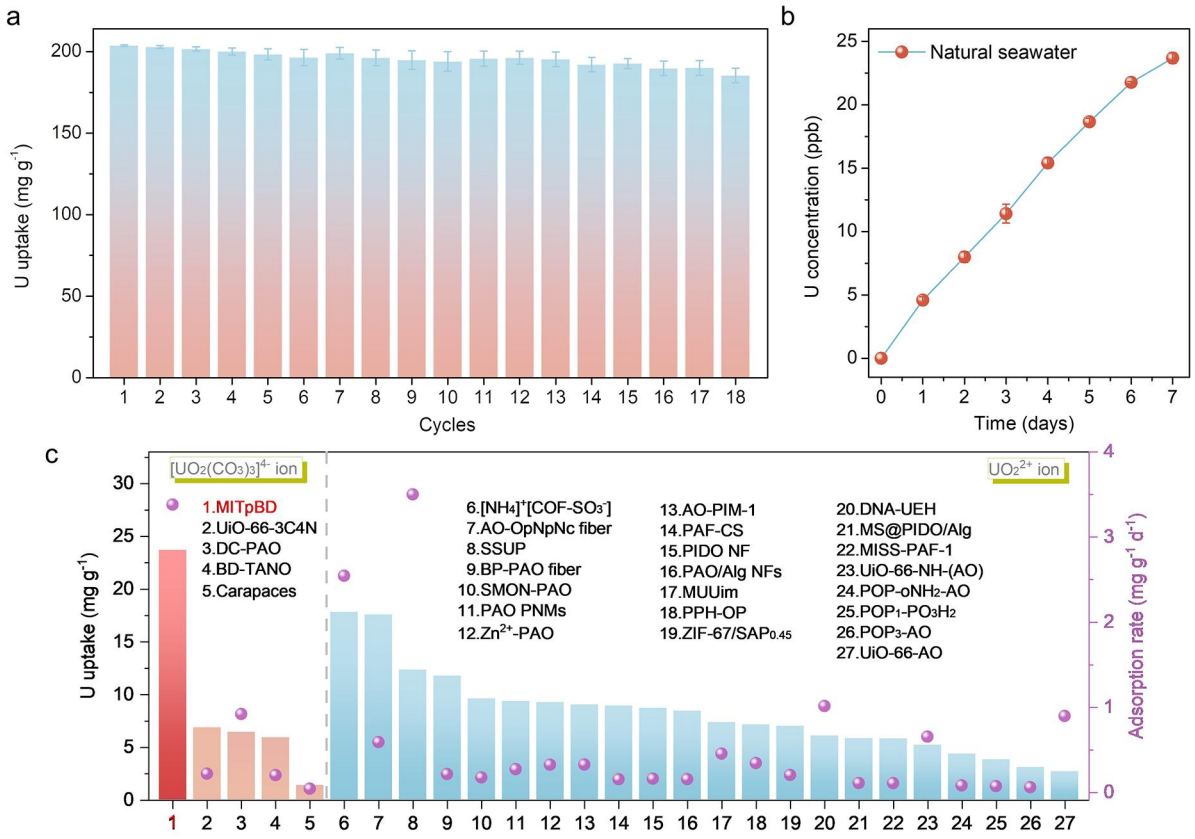


Fig. 5 | Uranium recovery and uptake from real seawater. a, Recycling experiment of MITpBD (initial uranium concentration ≈ 10 ppm). **b,** Uranium adsorption performance of MITpBD during 7 days of close contact in natural seawater (initial uranium concentration ≈ 3.4 ppb). Error bars represent the standard deviation obtained from three independent measurements. **c,** Comparison of the adsorption capacities and adsorption rates of all adsorbents reported (initial concentration of uranium is 3–3.4 ppb in natural seawater). The values are plotted as-is from reported references, and the specific adsorption values for each sample (1–27) are listed in Supplementary Table 13.

Conclusions

In conclusion, we have developed a multiple-dynamic-bonds strategy by modulating the pore size and environment COF networks. After introducing multiple hydroxyl groups in COF channels with a pore size of 0.6–2.5 nm, five hydroxy-rich COFs were synthesized and used for capturing uranium from the aquatic environment. Through synergistic electrostatic (ammonium cations) and hydrogen-bonding (hydroxyl groups) interactions, the resulting solid achieved an ultrahigh saturated adsorption uptake of 800.0 mg^{-1} in a 10 ppm uranium-spiked solution and exhibited a fast uranium-extraction rate with the removal rate of 99.99% within 400 min. In particular, a record uranium adsorption uptake of 23.68 mg g^{-1} was realized within 7 days of exposure to natural seawater. This study addressed the low kinetics in the dissociation of CO_3^{2-} ions from uranyl tricarbonate ions and provided a new direction to develop fast-kinetics, high-affinity, and applicable adsorbents for uranium capture.

Methods

Preparation of the $[UO_2(CO_3)_3]^{4-}$ anion imprinted complex (MIC). The $[UO_2(CO_3)_3]^{4-}$ anion imprinted complex (MIC) was prepared by mixing trimesic acid and glycidol into ethanol (10 mL). After stirring the solution at 298 K for 4 h, the solvent was removed from the system under a vacuum. Finally, the MIC powder was dried under a vacuum at 298 K for 4 h.

Synthesis of TpHz, TpPaOH, TpBDOH. The detailed synthetic procedure of COF solids (i.e., TpHz, TpPaOH, and TpBDOH) is provided in the literature[24–26]. In a typical synthesis, a pyrex tube (outer diameter × inner diameter = 10 mm × 8 mm, length = 18 cm) was poured with 0.3 mmol 1,3,5-triformylphloroglucinol (Tp) and 0.45 mmol corresponding diamine monomers

(hydrazine hydrate (Hz), 2,5-diaminobenzene-1,4-diol dihydrochloride (PaOH), or 3,3-dihydroxybenzidine (BDOH)), 1.5 mL of mesitylene, 1.5 mL of 1,4-dioxane, and 0.5 mL of 3 M acetic acid. This mixture was sonicated for 10 min to obtain a uniformly dispersed liquid. The tube was flash-frozen at 77 K in an N_2 bath and degassed via three freeze−pump−thaw cycles. Then, the tube was heated at 393 K for 72 h. After cooling the tube to 298 K, a solid powder was obtained by filtration and washed three times with methanol, tetrahydrofuran, and acetone. Finally, the COF powder was dried under a vacuum at 393 K for 12 h.

Synthesis of MITpPa and MITpBD. MITpPa and MITpBD powders were prepared using a similar procedure. For MITpBD, 0.25 g of the MIC and 25 mL of anhydrous ethanol were added to a 50-mL Teflon-lined stainless steel autoclave and stirred for 2 h. Then, 0.4 g of the TpBDOH powder was added to this solution and uniformly dispersed under sonication. After heating the solution at 353 K for 24 h, a solid powder was obtained via filtration and washed with ethanol to remove the unreacted glycidol. The filtrate was transferred to a 100-mL volumetric flask, and 100 mL of ethanol was added to the powder. The mixture was stirred for 6 h and vacuum-assisted filtration was performed to obtain the resulting COF solid. Finally, the powder was vacuum-dried at 393 K for 12 h[27].

Uranium adsorption as a function of the initial UO_2^{2+} concentrations. 5 mg of each COF sample was added to 500 mL of ammonium uranyl tricarbonate solutions with concentrations ranging from 2 to 150 ppm. After stirring for 720 min, 1 mL of the solution was sampled using a syringe. The concentration of the solution was determined using a UV spectrophotometer and *Beer–Lambert law*, according to Equation (1).

$$A = \log\frac{1}{T} = Kbc \qquad (1)$$

where A is the absorbance of the solution, T is the transmittance of the solution, K is the molar absorption coefficient, b is the thickness of the absorbing layer, and c is the concentration of the substrate. Using arsenazo as the imaging agent, 0.5 mL of the solution was poured into a mixture of 1 mL of azoarsenic (500 mg L^{-1}) and 0.25 mL of HCl (0.1 mol L^{-1}), followed by dilution with 3.25 mL of water.

The adsorption uptake of the COF sample was calculated using Equation (2):

$$q_e = \frac{(C_0 - C_e) \times V}{m} \qquad (2)$$

where C_0 and C_e (mg L^{-1}) are the uranium concentrations in the initial and equilibrium states, respectively; V (L) is the solution volume; m (g) is the weight of the COF powder; and q_e (mg g^{-1}) is the adsorption uptake.

The adsorption uptake curves of the COF sample at different concentrations were fit using *Langmuir* and *Freundlich* models.

Langmuir model:

$$\frac{C_e}{q_e} = \frac{1}{k_L q_{max}} + \frac{C_e}{q_{max}} \qquad (3)$$

Freundlich model:

$$\ln q_e = \ln K_F + \frac{1}{n} C_e \qquad (4)$$

where C_e (mg L^{-1}) is the equilibrium concentration of the material, q_e (mg g^{-1}) is the equilibrium adsorption uptake, q_{max} (mg g^{-1}) is the maximum adsorption uptake, and k_L and k_f (L mg^{-1}) are the *Langmuir* and *Freundlich* binding constants, respectively.

Scandium(III) adsorption kinetics. 5 mg of each COF sample was added to 500 mL of an ammonium uranyl tricarbonate solution with a concentration of ~10 ppm. After stirring the solution for 720 min, 1 mL of the solution was sampled at various time intervals using a syringe. The concentration of the solution was determined using a UV spectrophotometer and *Beer–*

Lambert law, according to Equation (1). The adsorption kinetic data were fitted by the *pseudo-first-order* and *pseudo-second-order* models.

Pseudo-first-order model:

$$\log (Q_e - Q_t) = \log Q_e - \frac{k_1}{2.303} t \qquad (5)$$

Pseudo-second-order model:

$$\frac{t}{Q_t} = \frac{1}{k_2 \times Q_e^2} + \frac{1}{Q_e} \qquad (6)$$

where Q_t (mg·g^{-1}) is the adsorption uptake of the COF sample at time t (min), Q_e (mg g^{-1}) is the equilibrium adsorption uptake of the COF sample, and k_1 and k_2 (mg·mg^{-1}·min^{-1}) are the *pseudo-first-order* and *pseudo-second-order* kinetics constants, respectively.

Distribution coefficient. 1 mg of each COF sample was added to 50 mL of an ammonium uranyl tricarbonate solution with a concentration of ~5 ppm. After stirring for 720 min, 1 mL of the solution was sampled at various time intervals using a syringe. The concentration of the solution was determined using a UV spectrophotometer and *Beer–Lambert law*, according to Equation (1). The distribution coefficient is calculated using Equation (7).

$$K_d = \frac{C_0 - C_t}{C_t} \times \frac{V}{m} \qquad (7)$$

where C_0 and C_e (mg L^{-1}) are the initial and equilibrium concentrations of the COF sample, respectively; V (L) is the volume of the solution; and m (g) is the weight of the adsorbent.

Selectivity studies. 5 mg of MITpBD was added to 500 mL of a solution containing 3 ppm each of $[UO_2(CO_3)_3]^{4-}$, Na^+, K^+, VO_2^+, Mg^{2+}, Ca^{2+}, Cd^{2+}, Ni^{2+}, Cu^{2+}, Zn^{2+}, and Fe^{3+}. After stirring for 24 h, the concentrations of metal ions were determined using an inductively coupled plasma-atomic emission spectrometer. The selectivity coefficient ($K_{U/M}$) was calculated using Equation (8):

$$K_{U/M} = \frac{Q_U}{Q_M} \times 100\% \quad (8)$$

where Q_U and Q_M (mg g^{-1}) are the concentrations of uranium and other metal ions adsorbed, respectively.

Cycling experiments. 5 mg of each COF sample was added to 500 mL of an ammonium uranyl tricarbonate solution with a concentration of ~10 ppm. After stirring for 720 min, 1 mL of the solution was sampled at various time intervals using a syringe. The concentration of uranium ion was determined using a UV spectrophotometer and according to *Beer–Lambert law* via Equation (1). The MITpBD adsorbent was recovered via centrifugation and washed with a 0.1 mol L^{-1} Na_2CO_3 solution for 30 min to remove uranium ions. The washing steps were repeated three times, and the MITpBD powder was collected via filtration and dried under a vacuum at 373 K for 12 h for the next adsorption.

Uranium uptake from natural seawater. 5 mg of MITpBD was added to 25 mL of 1 mol L^{-1} ammonium chloride and stirred for 12 h. Then, the COF sample was isolated via filtration; the ammonium cation–adsorbed MITpBD sample was charged to 100 L of natural seawater with a concentration of ~3.4 ppb. At interval times of 1, 2, 3, 4, 5, 6, and 7 d, the uranium ion uptake of MITpBD was recorded via inductively coupled plasma mass spectrometry.

Data availability

The authors declare that the main data supporting the findings of this study are available within the article and its Supplementary Information files. Extra data are available from the corresponding author upon request.

References

1. *Uranium 2020* (NEA, IAEA, 2021).
2. Rhodes, R. More nuclear power can speed CO_2 cuts. *Nature* **548**, 281 (2017).
3. Wu, Y. *et al.* Functional nanomaterials for selective uranium recovery from seawater, material design, extraction properties and mechanisms. *Coordin*. *Chem*. *Rev*. **483**, 215097 (2023).
4. Lindner, H. & Schneider, E. Review of cost estimates for uranium recovery from seawater. *Energ*. *Econ*. **49**, 9–22 (2015).
5. Xiong, X. *et al.* Ammoniating covalent organic framework (COF) for high-performance and selective extraction of toxic and radioactive uranium ions. *Adv*. *Sci*. **6**, 1900547 (2019).
6. Lashley, M. A. *et al.* Highly preorganized ligand 1, 10-phenanthroline-2, 9-dicarboxylic acid for the selective recovery of uranium from seawater in the presence of competing vanadium species. *Inorg*. *Chem*. **55**, 20 (2016).
7. Liu, Z. *et al.* Anti-biofouling and water-stable balanced charged metal organic framework-based polyelectrolyte hydrogels for extracting uranium from seawater. *ACS Appl*. *Mater*. *Interfaces* **12**, 18012–18022 (2020)
8. Liu, C. *et al.* A half-wave rectified alternating current electrochemical method for uranium extraction from seawater. *Nat*. *Energy* **2**, 1–8 (2017).
9. Cui, W. *et al.* Low band gap benzoxazole‐linked covalent organic frameworks for photo‐enhanced targeted uranium recovery. *Small* **17**, 2006882 (2021).
10. Wang, Z. *et al.* Constructing an ion pathway for uranium extraction from seawater. *Chem* **6**, 1683–1691 (2020).
11. Sun, Q. *et al.* Bio-inspired nano-traps for uranium extraction from seawater and recovery from nuclear waste. *Nat*. *Commun*. **9**, 1–9 (2018).

12. Mason, C. F. V. *et al.* Carbonate leaching of uranium from contaminated soils. *Environ*. *Sci*. *Technol*. **31**, 2707–2711 (1997).

13. Santos, E. A. & Ladeira, A. C. Q. Recovery of uranium from mine waste by leaching with carbonate-based reagents. *Environ*. *Sci*. *Technol*. **8**, 3591–3597 (2011).

14. Kaushik, A. *et al.* Large-area self-standing thin film of porous hydrogen-bonded organic framework for efficient uranium extraction from seawater. *Chem* **8**, 2749–2765 (2022).

15. Wang, Y. *et al.* Adsorption of U (VI) from aqueous solution by the carboxyl-mesoporous carbon. *Chem*. *Eng*. *J*. **198**, 246–253 (2012).

16. Chen, D. *et al.* Bio-inspired functionalization of electrospun nanofibers with anti-biofouling property for efficient uranium extraction from seawater. *Chem*. *Eng*. *J*. **465**, 142844 (2023).

17. Song, Y. *et al.* Nanospace decoration with uranyl-specific "hooks" for selective uranium extraction from seawater with ultrahigh enrichment index. *ACS Cent*. *Sci*. **7**, 1650–1656 (2021).

18. Feng, L. *et al.* In situ synthesis of uranyl-imprinted nanocage for selective uranium recovery from seawater. *Angew*. *Chem*. *Int*. *Ed*. **134**, e202101015 (2022).

19. Guo, X. *et al.* DFT investigations of uranium complexation with amidoxime-, carboxyl-and mixed amidoxime/carboxyl-based host architectures for sequestering uranium from seawater. *Inorg*. *Chim*. *Acta* **441**, 117–125 (2016).

20. Gan, J. *et al.* Phosphorylation improved the competitive U/V adsorption on chitosan-based adsorbent containing amidoxime for rapid uranium extraction from seawater. *Int*. *J*. *Biol*. *Macromol.* **238**, 124074 (2023).

21. Wang, Z. *et al.* Constructing uranyl-specific nanofluidic channels for unipolar ionic transport to realize ultrafast uranium extraction. *J*. *Am*. *Chem*. *Soc*. **143**, 14523–14529 (2021).

22. Wang, D. *et al.* Significantly enhanced uranium extraction from seawater with mass produced fully amidoximated nanofiber adsorbent. *Adv*. *Energy Mater*. **8**, 1802607 (2018).

23. Yuan, Y. *et al.* Rational design of porous nanofiber adsorbent by blow-spinning with ultrahigh uranium recovery capacity from seawater. *Adv*. *Funct*. *Mater*. **29**, 1805380 (2019).

24. Chandra, S. *et al.* Molecular level control of the capacitance of two-dimensional covalent organic frameworks, role of hydrogen bonding in energy storage materials. *Chem*. *Mater*. **29**, 2074–2080 (2017).

25. Maia, R. A. *et al.* Crystal engineering of covalent organic frameworks based on hydrazine and hydroxy-1, 3, 5-triformylbenzenes. *Cryst*. *Growth Des*. **18**, 5682–5689 (2018).

26. Yi, S. *et al.* Ionic liquid modified covalent organic frameworks for efficient detection and adsorption of ReO_4^-/TcO_4^-. *J. Environ*. *Chem*. *Eng*. **10**, 107666 (2022).

27. Jiang, Y. *et al.* Stainless-steel-net-supported superhydrophobic COF coating for oil/water separation. *J*. *Membrane Sci*. **587**, 117177 (2019).

28. Mu, Z. *et al.* Zwitterionic covalent organic frameworks as catalysts for hierarchical reduction of CO_2 with amine and hydrosilane. *ACS Appl*. *Mater*. *Interfaces* **10**, 41350–41358 (2018).

29. Yuan, Y. *et al.* Molecularly imprinted porous aromatic frameworks and their composite components for selective extraction of uranium ions. *Adv*. *Mater*. **30**, 1706507 (2018).

30. Zeppuhar, A. N. *et al.* Linkage transformations in a three-dimensional covalent organic framework for high-capacity adsorption of perfluoroalkyl substances. *ACS Appl*. *Mater*. *Interfaces* **15**, 28476–28490 (2023).

31. Gao, S. *et al.* Covalent organic framework membrane with angstrom discrimination in pore size for highly permselective ionic liquid nanofiltration. *ACS Sustain*. *Chem*. *Eng*. **11**, 15910–15918 (2023).

32. Halder, A. *et al.* Ultrastable imine-based covalent organic frameworks for sulfuric acid recovery, an effect of interlayer hydrogen bonding. *Angew*. *Chem*. *Int*. *Ed*. **57**, 5797–5802 (2018).

33. Chen, D. *et al.* Bio-inspired functionalization of electrospun nanofibers with anti-biofouling property for efficient uranium extraction from seawater. *Chem*. *Eng*. *J*. **465**, 142844 (2023).

34. Yuan, Y. *et al.* Rational design of porous nanofiber adsorbent by blow-spinning with ultrahigh uranium recovery capacity from seawater. *Adv. Funct. Mater*. **29**, 1805380 (2019).

35. Zhang, D. *et al.* Highly efficient extraction of uranium from seawater by polyamide and amidoxime co-functionalized MXene. *Environ*. *Pollut*. **317**, 120826 (2023).

36. Liang, Y. *et al.* Guanidinium-based ionic covalent organic frameworks for capture of uranyl tricarbonate. *Adv*. *Compos*. *Hybrid Ma*. **5**, 184–194 (2022)

37. Yuan, Y. *et al.* A bio-inspired nano-pocket spatial structure for targeting uranyl capture. *Angew*. *Chem*. *Int*. *Ed*. **59,** 4262–4268 (2020).

38. Zhong, X. *et al.* The role of functional-group-tuning in adsorption-photoreduction of U (VI) onto β-ketoenamine covalent organic frameworks photosystem. *Chem*. *Eng*. *J*. **467**, 143415 (2023).

39. Qiu, J. *et al.* Porous covalent organic framework based hydrogen-bond nanotrap for the precise recognition and separation of gold. *Angew*. *Chem*. *Int*. *Ed*. **135**, e202300459 (2023).

40. Shi, Y. *et al.* Anchoring LiCl in the nanopores of metal-organic frameworks for ultra-high uptake and selective separation of ammonia. *Angew*. *Chem*. *Int*. *Ed*. **61**, 202212032 (2022).

41. Chandra, S. *et al.* Molecular level control of the capacitance of two-dimensional covalent organic frameworks, role of hydrogen bonding in energy storage materials. *Chem*. *Mater*. **29**, 2074–2080 (2017).

42. Lohse, M. S. *et al.* Sequential pore wall modification in a covalent organic framework for application in lactic acid adsorption. *Chem*. *Mater*. **28**, 626–631 (2016).

43. Zhou, L. *et al.* Suppressing hydrogen evolution in aqueous lithium-ion batteries with double-site hydrogen bonding. *ACS Energy Lett*. **8**, 40–47 (2022).

44. Swanson, H. L. *et al.* Probing the binding modes and dynamics of histidine on fumed silica surfaces by solid-state NMR. *Phys*. *Chem*. *Chem*. *Phys*. **22**, 20349–20361 (2022).

45. Xiong, X. *et al.* Ammoniating covalent organic framework (COF) for high‐performance and selective extraction of toxic and radioactive uranium ions. *Adv*. *Sci*. **6**, 1900547 (2019).

46. Xu, X. *et al.* Ultrahigh and economical uranium extraction from seawater via interconnected open-pore architecture poly(amidoxime) fiber. *J*. *Mater*. *Chem*. *A* **8**, 22032–22044 (2020).

47. Yuan, Y. *et al.* Ultrafast and highly selective uranium extraction from seawater by hydrogel-like spidroin-based protein fiber. *Angew*. *Chem*. *Int*. *Ed*. **131**, 11911–11916 (2019).

48. Wang, N. *et al.* Accelerated chemical thermodynamics of uranium extraction from seawater by plant‐mimetic transpiration. *Adv*. *Sci*. **8**, 2102250 (2021).

49. Mei, D. & Yan, B. β-Ketoenamine and benzoxazole-Linked covalent organic frameworks tailored with phosphorylation for efficient uranium removal from contaminated water systems. *Adv*. *Funct*. *Mater*. **4**, 2313314–2313326 (2023).

50. Feng, X. *et al.* Highly efficient extraction of uranium from seawater by natural marine crab carapace. *Chem*. *Eng*. *J*. **430**, 133038 (2022).

Acknowledgements

G.Z. was supported by the National Key R&D Program of China (Grant No. 2022YFB3805902), the National Natural Science Foundation of China (Grant Nos. 22131004 and U21A20330), and the "111" project (Grant No. B18012). Y. Yuan was supported by the National Natural Science Foundation of China (Grant Nos. 21975039 and 22322501), the Fundamental Research Funds for

the Central Universities (Grant Nos. 2412020ZD008 and GFPY202309), and the CNNC Key Laboratory on Uranium Extraction from Seawater (KLUES202202). Y. Yang was supported by the National Natural Science Foundation of China (Grant No. 52204389).

Author contributions

Y.Yuan and D.C. contributed equally. D.C. carried out the experiments and performed the data interpretation. F.C. and C.Z. conducted the theoretical calculations. Y.Yang helped design the experiments and wrote portions of the manuscript. Y.S., Y.Z., S.C., Y.S., and F.W. performed the characterizations for uranium adsorption. Y.Y. and G.Z. developed the concept, supervised the experiments and drafted the manuscript.

Competing interests

The authors declare no competing financial interests.

Additional information

Supplementary information The online version contains supplementary material available at

Correspondence and requests for materials should be addressed to Guangshan Zhu.

Peer review information Nature Water thanks the anonymous reviewers for their contribution to the peer review of this work.

Reprints and permissions information is available at www.nature.com/reprints.

Publisher's note Springer Nature remains neutral with regard to jurisdictional claims in published maps and institutional afiliations.

Supplementary Files

This is a list of supplementary files associated with this preprint. Click to download.

- SIU.pdf